scientific reports

Check for updates

OPEN

Rapid detection of airborne fungal contamination using a molecularly imprinted polymer approach for ergosterol

Eun-Sook Choi[1], Jung-Hee Kim[1], Yun-Cheol Na[2], Bong Gu Lee[3], Min-Kyeong Yeo[3] & Eunjoo Kim[1]✉

Fungi are major biological contaminants in indoor air, and their concentration is typically assessed using the culture-based CFU method, which is labor-intensive and time-consuming. Ergosterol, a major fungal cell membrane component, has emerged as a preferred target for alternative analytical approaches. However, ergosterol is highly hydrophobic, and specific affinity probes such as antibodies or aptamers have not yet been successfully developed. In this study, we fabricated ergosterol-specific probes using molecularly imprinted polymers (MIPs) immobilized on carbon nanotubes (CNTs) and integrated them into a screen-printed electrode (SPE) platform. Surface polymerization was initiated through a thiol-ene click reaction using pentaerythritol tetrakis(3-mercaptopropionate) (PETMP) and glyoxal bis(diallyl acetal) (GO), which were selected based on predicted stable conformations for MIP synthesis. The resulting MIP@CNT sensor achieved an imprinting factor (IF) of 19.26 and a limit of detection (LOD) of 0.22 pM for ergosterol. Ergosterol levels in indoor air samples collected on PVC filters were quantified using the MIP@CNT sensor and showed significant correlation with GC/MS measurement ($R^2 = 0.5136$, $p < 0.0001$), moderate but statistically significant correlation. This work provides a valuable reference for developing sensing platforms for highly hydrophobic molecules such as sterols and phytosterols, which represent important analytical targets in environmental and biological monitoring.

Keywords Molecularly imprinted polymer, Ergosterol, Screen-printed electrode, Fungi, Indoor air

Efficient detection of airborne fungi is essential for the indoor air quality management and protection of human health. Current monitoring approaches can be broadly categorized into culture-based and culture-independent methods. The traditional colony-forming unit (CFU) method quantifies viable fungal spores capable of forming colonies on specific media[1,2]. Although this approach is widely used in governmental and industrial sectors, it has notable limitations, including long turnaround times (2–4 days), limited sensitivity, and the inability to detect non-viable fungi that remain potential sources of harmful bioactive components such as endotoxins.

Culture-independent detection is performed by measuring specific fungal biomarkers. Ergosterol is a representative marker for fungi to determine their concentration in ambient air[3,4] because it is vital for maintaining the structure, fluidity, and permeability of fungal membranes[5,6]. To measure ergosterol, chromatographic or spectroscopic methods have been employed, such as gas chromatography (GC) and high-performance liquid chromatography (HPLC)[7–9]. However, these approaches require specialized equipment and long analysis times (from hours to days), which do not satisfy the need for rapid and cost-effective environmental monitoring. To overcome these challenges, the direct detection and quantification of ergosterol in air samples using sensing techniques could be an efficient monitoring method. In this case, specific detection probes are required to bind ergosterol in complex mixtures sampled from indoor air.

Until now, most probes used in biosensors have focused on antibodies or aptamers due to their three-dimensional conformation, which allows them to bind target ligands specifically. This binding typically involves ionic interactions, hydrogen bonds, and partially van der Waals interactions[10]. However, ergosterol is a highly

[1]Division of ABB Research, Daegu Gyeongbuk Institute of Science and Technology (DGIST), Techno-jungangdaero 333, Dalsung-gun, Daegu 42988, Republic of Korea. [2]Metropolitan Seoul Center, Korea Basic Science Institute (KBSI), Seoul 03759, Republic of Korea. [3]Department of Environmental Science and Engineering, Kyung Hee University, Yougin 44670, Republic of Korea. ✉email: ejkim@dgist.ac.kr

hydrophobic material, and therefore, it is not expected to exhibit sufficient hydrophilic affinity for antibody or aptamer probes.

In this study, we prepared newly developed probes for ergosterol using molecularly imprinted polymers (MIPs). MIPs detect ergosterol primarily based on the hydrophobic van der Waals interactions that occur between hydrocarbon monomers and ergosterol[11]. After polymerization, the template is removed, leaving behind cavities that are complementary in shape, size, and functional groups to the target molecule[12]. This preparation method is cost-effective[13] and can be integrated into various detection platforms, including electrochemical, optical, and spectroscopic systems[14,15]. A recent study has demonstrated the integration of MIPs with optical sensing platforms[16,17] or nanomaterials[18] to achieve sensitive and selective detection of target analytes in complex samples.

In this study, electrochemical signals were analyzed using gold screen-printed electrodes (SPEs) covered with MIP-immobilized carbon nanotubes (MIP@CNT) specific for ergosterol. CNTs were incorporated as a supporting material for MIPs to enhance electrical conductivity, increase surface area, and provide initiation sites for polymerization. To immobilize MIPs on the CNT surface, thiol-ene click chemistry was performed to functionalize the CNT surface using a reagent with multiple thiol groups, pentaerythritol tetrakis(3-mercaptopropionate) (PETMP). Additionally, to create more abundant sites for molecular imprinting, glyoxal bis(diallyl acetal) (GO) was further incorporated onto the PETMP-modified CNT surface, based on the analysis of the compounds' stabilized conformation. Then, the imprinting of ergosterol was conducted with methyl methacrylate (MMA) as the active site functional monomer, and ethylene glycol dimethacrylate (EGDMA) and GO as cross-linking agents.

In this work, we introduced a polymerization strategy that used PETMP–GO dual anchors by thiol-ene click chemistry to construct CNT-supported MIPs as specific probes for ergosterol detection. The dual-anchoring approach provided diverse attachment sites and probe conformations in the polymer matrix, enabling the formation of specific recognition cavities in imprinted polymers. Compared with previously reported MIP sensors, this design increases the number and diversity of molecular recognition sites, thereby enhancing binding affinity and detection limit performance.

The effectiveness of the compound selection in this study was supported by the resulting MIP@CNT sensor characterization, as confirmed by the improved binding properties. In addition, the ergosterol concentration in indoor air samples collected on PVC filters was analyzed using the MIP@CNT sensor and compared with that of conventional GC/MS analysis. Overall, our study using an MIP-based sensing platform for ergosterol proposes an expanded reagent option for molecular imprinting and offers an alternative method to evaluate biological contamination by fungi originating from indoor air.

Methods

Reagents

Single-walled CNTs (SWCNT, IsoNanotubes-S 99%) were obtained from Nanointegris Technology (Skokie, IL, USA). PETMP, GO, ergosterol, MMA, and EGDMA were purchased from Sigma-Aldrich (Saint Louis, MO, USA). Electrocatalysts, potassium ferricyanide ($K_3[Fe(CN)_6]$, Fe(III)), and potassium ferrocyanide trihydrate ($K_4[Fe(CN)_6]\cdot 3H_2O$, Fe(II)), along with the radical initiator azobisisobutyronitrile (AIBN), were also purchased from Sigma-Aldrich.

Preparation of ergosterol MIP probes immobilized on CNT by molecular imprinting of ergosterol

The CNT film (0.5 × 0.5 cm) was dispersed in 1 mL of dimethylformamide (DMF, Sigma-Aldrich) and sonicated for 60 min, followed by centrifugation at 15,000 × *g* for 30 min. A total of 500 µL of the upper phase was collected, and 500 µL of acetonitrile was added. To this CNT suspension, 20 µL of 1 mM PETMP in acetonitrile was added dropwise. The mixture was then exposed to UV light (60 W) for 30 min to produce P-CNTs (Fig. 1). Unreacted PETMP was washed away via ultrafiltration using a 3,000 MW Amicon® Ultra centrifuge filter (MilliporeSigma, Burlington, MA, USA). The filtered P-CNT particles were dispersed in 1 mL DMF. To modify the CNT surface with multiple polymerizable sites for ergosterol binding, 20 µL of 1 mM GO in acetonitrile was additionally linked to P-CNTs via UV irradiation for 30 min to produce PG-CNTs (Fig. 1). Unreacted GO was washed by ultrafiltration with a 3,000 MW Amicon® Ultra centrifuge filter (MilliporeSigma). The filtered PG-CNT particles were dispersed in 1 mL DMF. To form a template-functional monomer complex for the molecular imprinting of ergosterol, a solution of 1 mM ergosterol and 4 mM MMA in acetonitrile was prepared and pre-incubated at a molar ratio of 1:4 at 55 °C for 15 min. For assessing the non-specific binding of ergosterol to polymers, an MMA solution without a template was prepared to synthesize non-imprinted polymer (NIP) probes on the CNT surface (NIP@CNT). To polymerize the template-monomer complex onto the CNT substrate, the incubated mixture was added to the PG-CNT suspension, and crosslinking reagents were mixed to reach final concentrations of 10 mM EGDMA, 10 mM GO, 1 mM toluene, and 0.2 mM AIBN. Polymerization was carried out for 6 h at 60 °C following a 20-minute purge with N_2. The unreacted materials were washed away using ultrafiltration with a 3000 MW centrifuge filter.

After polymerization, the removal of ergosterol templates bound to the MIPs was performed. The solution was centrifuged at 15,000 × *g* for 10 min, and the pellet was dispersed in absolute ethanol. This suspension was then sonicated in a bath sonicator for 30 min to remove templates. Finally, the solution was centrifuged again at 15,000 × *g* for 10 min, and the pellet was resuspended in DMF to produce the final ergosterol MIP@CNT probes. The exact process was used to prepare NIP@CNT, using MMA without preincubation of ergosterol.

The MIP@CNT and NIP@CNT suspension (1 µL each) was dropped onto the working electrode of the gold SPE chip (C220AT, Metrohm DropSens, Asturias, Spain). After drying at room temperature, the MIP@CNT

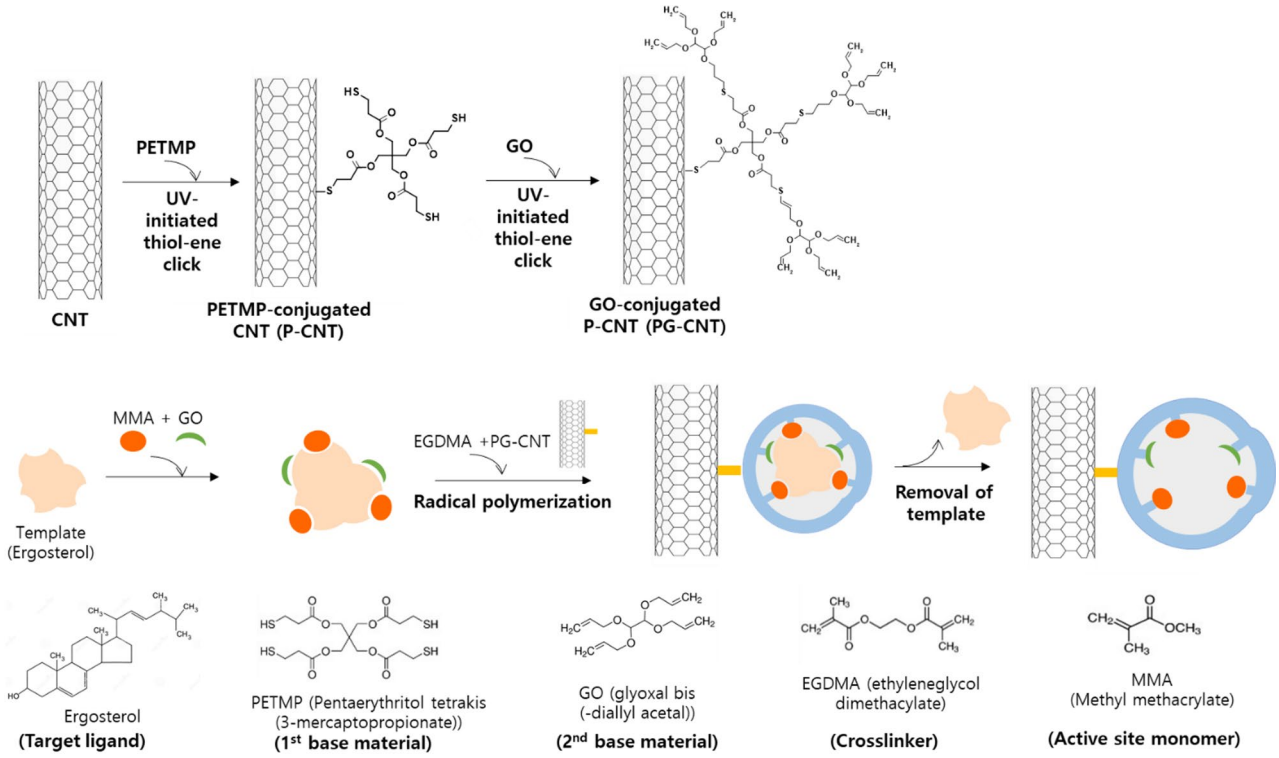

Fig. 1. Schematic illustration of the fabrication process of the MIP@CNT-modified gold SPE sensor. The sensing platform is based on PETMP–GO dual-anchoring chemistry for immobilizing the MIP layer onto CNTs.

sensor was used for ergosterol detection. A bare CNT sensor was also prepared to characterize the ergosterol-specific sensor by dropping the bare CNT suspension onto it.

Characterization of MIP@CNT probes

Transmission electron microscopy (TEM, Hitachi HF-3300, Tokyo, Japan) and scanning electron microscopy (SEM, Hitachi SU8020, Tokyo, Japan) were used to observe the morphology of MIP@CNTs and NIP@CNTs and to capture micrographs of the working electrode of SPE sensors. X-ray photoelectron spectroscopy (XPS, Thermo Scientific ESCALAB 250Xi, Waltham, MA, USA) was employed to analyze chemical modifications on the CNT surface. Using XPS, the polymerization reaction on CNT was confirmed by identifying atoms from the chemicals involved in MIP production. Fourier transform infrared absorption spectroscopy (FT-IR) was used to identify the chemical bonds in the synthesized polymer constructed on the CNT surface (Cary 5000 UV-Vis-NIR, Agilent Technologies, Waldbronn, Germany).

Measurement and analysis of electrochemical signals by ergosterol binding to the MIP@CNT sensor

Ergosterol concentration in various samples was measured using a potentiostat (μStat-i 400, Metrohm DropSens, Asturias, Spain). Before measuring electrochemical signals, the chip surface was thoroughly washed with phosphate-buffered saline (PBS). Then, 10 μL of the ergosterol samples were carefully dropped onto the working electrode of the MIP@CNT sensor and incubated for 10 min at 37 °C. After incubation, the chip surface was washed three times with PBS. Measurements were performed in the binding solution composed of a redox couple of 5 mM $K_3[Fe(CN)_6]/K_4[Fe(CN)_6]\cdot 3H_2O$ and 0.1 M KCl (1:1 v/v) in PBS.

Cyclic voltammetry (CV), electrochemical impedance spectroscopy (EIS), and SWV (square wave voltammetry) measurements were performed using μStat-i 400 potentiometer, and data acquisition and analysis of signals from bare CNT, NIP@CNT, and MIP@CNT sensors were carried out with DropView 8400 software (Metrohm DropSens, Asturias, Spain). The CV was scanned by cycling the potential between − 0.2 V and + 0.6 V at a scan rate of 50 mV/s, and the EIS analysis was conducted over frequencies ranging from 10^{-1} to 10^5 Hz at an amplitude of 50 mV. SWV measurements involved scanning from − 0.2 V to + 0.6 V with an amplitude of 2 mV and a frequency of 50 Hz.

The response of ergosterol binding to the MIP@CNT and NIP@CNT sensors was determined by normalizing the background signals through subtracting signals from the binding buffer and bare CNT modification. The binding response of ergosterol (R_E) at each concentration C to the SPE sensor was calculated using the following Eq. (1):

$$R_E = (R_{Sen\_C} - R_{Sen\_Zero}) - (R_{CNT\_C} - R_{CNT\_Zero}) \quad (1)$$

where R_{Sen_C} and R_{Sen_Zero} are the highest currents at the peak position of the SWV plot at concentration C and zero ergosterol concentration, respectively, and R_{CNT_C} and R_{CNT_Zero} are the SWV signals from bare CNT-modified SPE chips at concentrations C and zero, respectively. For preparing the ergosterol standard curve, concentration-dependent changes in SWV signals from the MIP@CNT sensor were calculated using the equation. The same equation was also used to determine the binding response to NIP@CNT.

Determination of the binding constant of ergosterol to the MIP@CNT sensor

The binding constant of ergosterol was determined using the Langmuir isotherm equation. The relationship between ergosterol concentration and the electrochemical signal from the MIP@CNT sensor was plotted using the following Eq. (2), which is the linear form of the Langmuir isotherm:

$$\frac{C}{R} = \frac{C}{R_{max}} + \frac{1}{(R_{max} \cdot K_A)} \tag{2}$$

where R is the background-corrected electrochemical signal measured by the potentiometer at ergosterol concentration C, R_{max} is the signal when C approaches infinity, and K_A is the association constant (M^{-1}).

Analysis of MIP@CNT specificity for ergosterol

To verify the specific binding of ergosterol to the MIP@CNT sensor, molecules with a similar structure and weight to ergosterol were applied to the sensor, β-sitosterol, stigmasterol, and cholesterol. The concentration of the competitors was increased from 0.1 pg/mL to 1 ng/mL for β-sitosterol and stigmasterol, and from 0.1 pg/mL to 100 pg/mL for cholesterol. Then the SWV electrochemical signals from the sensor were compared, using the same method described in "Measurement and analysis of electrochemical signals by ergosterol binding to the MIP@CNT sensor" section. To compare the responses of ergosterol and other sterols in the MIP sensor, changes in peak currents upon target treatment were determined by SWV analysis, as described in "Measurement and analysis of electrochemical signals by ergosterol binding to the MIP@CNT sensor" section.

Optimization of binding site regeneration and ergosterol binding conditions for MIP@CNT

To evaluate active-site regeneration in the MIP@CNT sensor for ergosterol detection, the template-removal efficiency of MIPs after polymerization was assessed. After synthesizing the probes through molecular imprinting of ergosterol, sonication in ethanol was carried out for 0, 15, and 30 min. The electrochemical signals from 0 to 0.1 ng/mL ergosterol were then measured using the SWV mode.

To evaluate the reusability of the MIP@CNT sensor, two consecutive SWV measurements were performed. The measurements were conducted for PBS solution without any analyte.

The binding conditions on the MIP@CNT sensor were optimized by varying the incubation temperature and time. The sensor signal was evaluated under two thermal conditions, 27 °C and 37 °C. For each temperature, the electrochemical response was measured after incubating 10 µL of the ergosterol sample on the working electrode for 1, 5, 10, and 30 min. After each incubation time, the sensor surface was washed three times with PBS to remove unbound molecules, and the peak current was measured using SWV as described in "Measurement and analysis of electrochemical signals by ergosterol binding to the MIP@CNT sensor" section.

Detection of ergosterol distributed in indoor air

A total of thirty sampling sites were arbitrarily chosen, including eight underground stations, five mega stores with dining services, ten underground parking lots, three kindergartens, and four libraries, all located in Seoul, Korea. During the days when indoor air samples were collected, seasonal and temporal variation was not considered. Indoor air samples for total particulate matter were obtained using indoor sampling pumps (Sensidyne, St. Petersburg, FL, USA), positioned at a height of 130 cm. The pumps, connected to 37-mm closed cassettes loaded with polyvinyl chloride (PVC) filters (pore size 5 µm, SKC, Inc., Eighty Four, PA, USA), operated at a flow rate of 4 L/min for 8 h. All equipment, materials, and supplies were sterilized before use. After sampling, the filters were placed in sterile filter containers and sealed with parafilm using sterile techniques. The sealed filters were then stored in a cooler with ice packs to maintain their cool temperature and minimize potential changes to the microbial community during transportation to the laboratory. All filter samples were stored at − 80 °C until analysis.

Ergosterol in the filtered air samples was analyzed after the extraction of biological contaminants from PVC filters. Each PVC filter was carefully placed into a 5 mL microtube containing 1 mL of 0.1× PBS buffer (pH 7.4) with 0.1% DMSO. The filter was then subjected to bead-beating using a microtube homogenizer (Benchmark Scientific, Sayreville, NJ, USA) for one minute. After homogenization, the disrupted filter material was removed by passing the solution through a 0.22 µm syringe filter. The resulting filtrates were stored at − 20 °C until further analysis.

For the GC/MS analysis of ergosterol in indoor air, a different PVC filter was prepared using the same sampling pump at the same locations of the collection sites. The filter was hydrolyzed for 3 h at 85 °C in 1 mL of methanolic hydrogen chloride solution. Ergosterol was then extracted from the hydrolyzed solution using 0.5 mL of hexane, and the extract was dried and reconstituted in 250 µL of a 1:1 (v/v) mixture of hexane and dichloromethane (DCM). The hydrolysate was loaded onto a Strata-Si solid-phase extraction cartridge (500 mg, Phenomenex, Torrance, CA, USA), which had been preconditioned with 1 mL of diethyl ether (DEE) followed by 1 mL of hexane: DCM (1:1, v/v). The cartridge was subsequently washed with 2 mL of a 1:1 (v/v) hexane: DCM mixture and 0.5 mL of DEE to remove impurities and concentrate the ergosterol. Ergosterol was then eluted with an additional 1.5 mL of DEE. As a surrogate standard, 7-dehydrocholesterol was added to the eluate, which was then dried and analyzed. Before instrumental analysis, the dried samples were derivatized to improve analyte

volatility and thermal stability, thereby enhancing chromatographic performance. Derivatization was performed by adding 50 µL of N, O-bis(trimethylsilyl)trifluoroacetamide (BSTFA) with 1% trimethylchlorosilane (TMCS) and 10 µL of pyridine, followed by heating at 85 °C for 1 h. The samples were subsequently evaporated to dryness and re-dissolved in 100 µL of hexane for the selected reaction monitoring (SRM) mode of GC/MS analysis. Analysis of ergosterol was carried out using an Agilent 7890B GC system (Agilent Technologies, Waldbronn, Germany) equipped with a DB-5MS column (30 m × 0.25 mm, 0.25 µm, J&W Scientific, Houston, TX, USA). Samples (1 µL) were injected in splitless mode at a flow rate of 1 mL/min. The oven temperature was programmed to increase from 80 to 300 °C at a rate of 15 °C/min and then held for 10 min. The separated compounds were analyzed on an Agilent 7010 triple quadrupole MS (Agilent Technologies, Waldbronn, Germany) with a 70 eV electron impact (EI) ionization source. Ergosterol and 7-dehydrocholesterol were quantified in multiple reaction monitoring (MRM) mode using transitions m/z 363 → 143 and m/z 351 → 143, respectively, with a collision energy of 20 eV.

Software

Simulation of the stable conformation of PETMP with cross-linked molecules of EGDMA and GO was performed using Scigress software (Version FQ 3.5.0, Fujitsu, Kanagawa, Japan). For the statistical analysis of the data, the curve fitness of the standard curve, the significance of Pearson's correlation, and the LOD determined by standard curve interpolation were calculated using Prism (Ver. 10.6.0, GraphPad Software, Boston, MA, USA).

Results and discussion

MIP-based ergosterol probes created on CNT surfaces through thiol-ene click chemistry

Figure 1 shows the process of molecular imprinting of ergosterol on the CNT surface to create MIP@CNT probes. PETMP was selected as the primary functional base material to introduce polymerizable sites onto the CNTs. This was achieved through a thiol-ene click reaction between the thiol groups of PETMP and the C = C bonds of the CNT, forming a covalent bond[19,20]. Since PETMP contains four thiol groups, it was initially hypothesized that it could anchor to the CNT while leaving multiple thiols available for subsequent crosslinking with other agents. However, in-silico simulation (Fig. 2) suggested that if three thiols participate in the click reaction with the CNT, only one thiol could remain capable of crosslinking with EGDMA. Therefore, GO was conjugated once more as a secondary base material via a second click reaction to increase the number of available crosslinking sites (Figs. 1 and 2). Finally, the pre-incubated ergosterol- MMA complex was conjugated onto the CNT surface through crosslinking with EGDMA and GO.

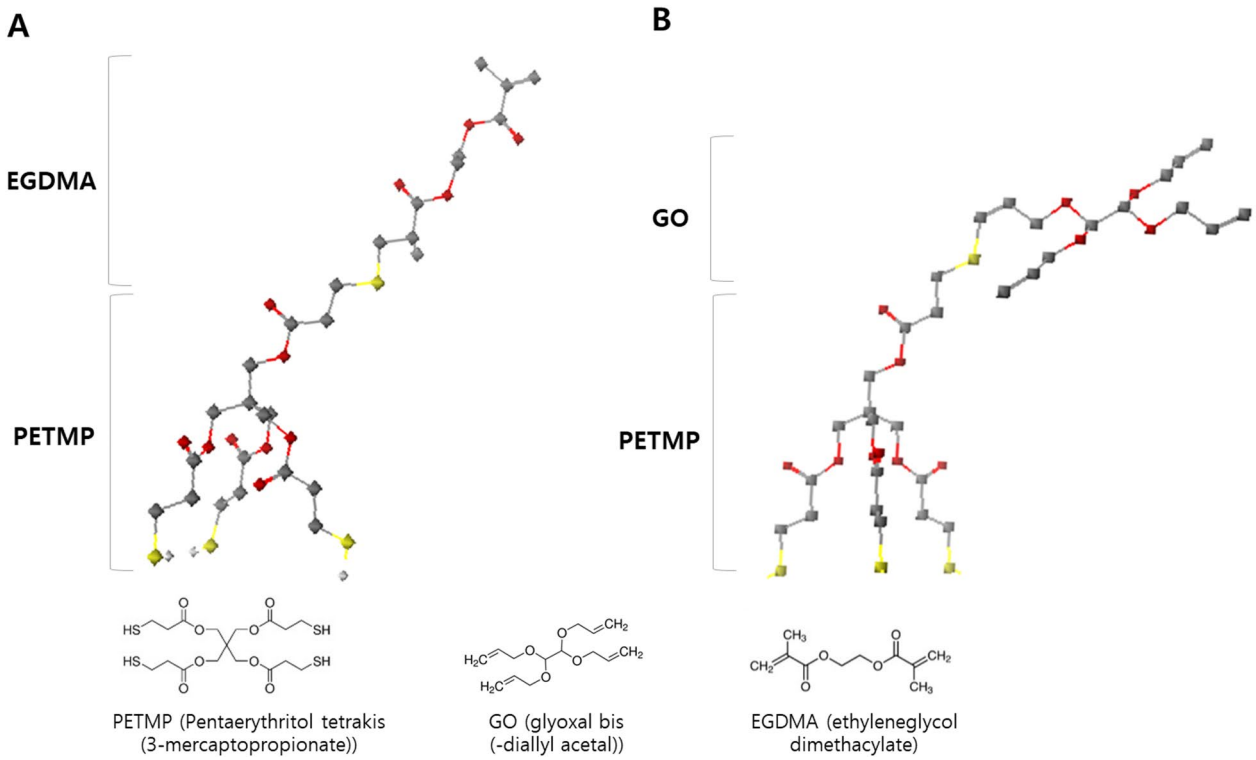

Fig. 2. Simulation of the stable conformation of PETMP with conjugated molecules. (**A**) PETMP-EGDMA conjugation and (**B**) PETMP-GO conjugation, using Scigress software (Version FQ 3.5.0, Fujitsu, Kanagawa, Japan). The simulation function verified valence, hybridization, hydrogen bonding, and geometry. Numbers in blue indicate the available sites for alkene groups to construct MIPs. By adding secondary basal material GO, the number of available sites for MIP synthesis can be increased.

The morphology of the synthesized probes was examined using TEM (Fig. 3, top). Both the NIP@CNT and MIP@CNT largely retained the structure of the bare CNTs. SEM analysis (Fig. 3, bottom) showed partial aggregation, but the overall morphology was preserved in both the NIP@CNT and MIP@CNT samples.

Furthermore, the atomic composition of the CNTs was clearly altered following the molecular imprinting, as shown by XPS analysis (Fig. 4). In the XPS spectra, a distinct peak for neutral sulfur (S 2p) was observed at a binding energy of 164 eV[21] in both NIP@CNT and MIP@CNT, which was absent in the bare CNTs. The S 2p peak observed in the XPS spectra originates from the sulfur-containing crosslinker PETMP used in the polymerization process. Since both NIP@CNT and MIP@CNT were prepared using the same PETMP-containing polymer system, the detected sulfur signal mainly reflects the presence of PETMP within the polymer matrix. The slight difference in S 2p peak intensity between the two samples may result from variations in polymer layer coverage or surface distribution during molecular imprinting. This observation confirms that the initial thiol-ene click reaction to anchor PETMP to the CNT surface was successful.

FT-IR spectroscopy was used to confirm the formation of the polymer layer on the CNT surface. The spectra of bare CNTs, NIP@CNTs, and MIP@CNTs are shown in Figure S2. Compared with bare CNTs, both NIP@CNTs and MIP@CNTs exhibited several additional absorption features, indicating the successful formation of polymers on the CNT surface. In Figure S2A, NIP@CNT and MIP@CNT displayed more pronounced absorption bands in the 2850–2950 cm^{-1} region, corresponding to aliphatic C–H stretching vibrations originating from the polymer backbone. These bands were much weaker in the bare CNT spectrum because CNTs mainly consist of graphitic carbons with limited aliphatic groups.

In the 1000–1100 cm^{-1} region, distinct absorption bands appear for NIP@CNTs and MIP@CNTs that can be assigned to C–O and C–O–C stretching vibrations, which are characteristic of ester linkages within the polymer derived from the crosslinkers and the monomers (Figure S2B). Overall, the appearance of polymer-related absorption bands in NIP@CNTs and MIP@CNTs, together with their absence or weaker intensity in bare CNTs, demonstrates the successful polymerization and modification of CNT surfaces with the NIP and MIP layers.

Electrochemical properties of SPE chips by the modification of imprinted and non-imprinted probes

The CV curve for the SPE sensors modified with MIP@CNT was measured by scanning voltage cycles between − 0.2 V and + 0.6 V at a scan rate of 50 mV/s. Figure 5A shows the CV curves comparing the bare CNT, NIP@CNT, and MIP@CNT-modified SPE chips; all plots exhibited well-defined reversible redox curves. The stepwise decrease in the peak current (I_p) from bare CNT to NIP@CNT and then to MIP@CNT indicates that the applied polymer layers served as physical barriers to electron diffusion on the sensor surface. Previous reports similarly noted that the addition of polymer films to electrodes typically results in a decrease in I_p[22,23]. The bare CNT-

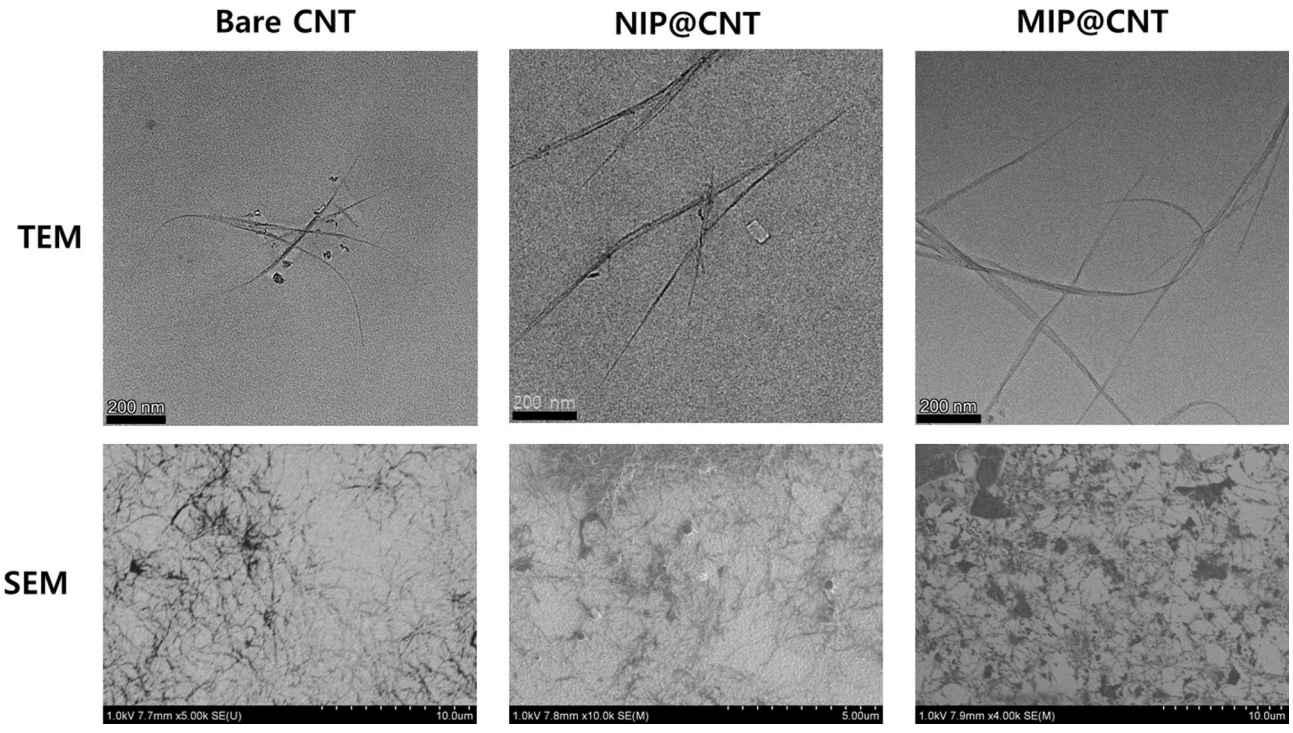

Fig. 3. Morphological structures of NIP@CNTs and MIP@CNTs compared to those of bare CNTs. (A) Morphology of CNTs dispersed in PBS was observed by transmission electron microscopy (TEM, top panel). (B) The distributed morphology of CNTs on the SPE chip was observed by scanning electron microscopy (SEM, bottom panel). In TEM images, the scale bar indicates 200 nm. For SEM images, magnifications of 5,000×, 10,000×, and 4000× were used for bare CNT, NIP@CNT, and MIP@CNT, respectively.

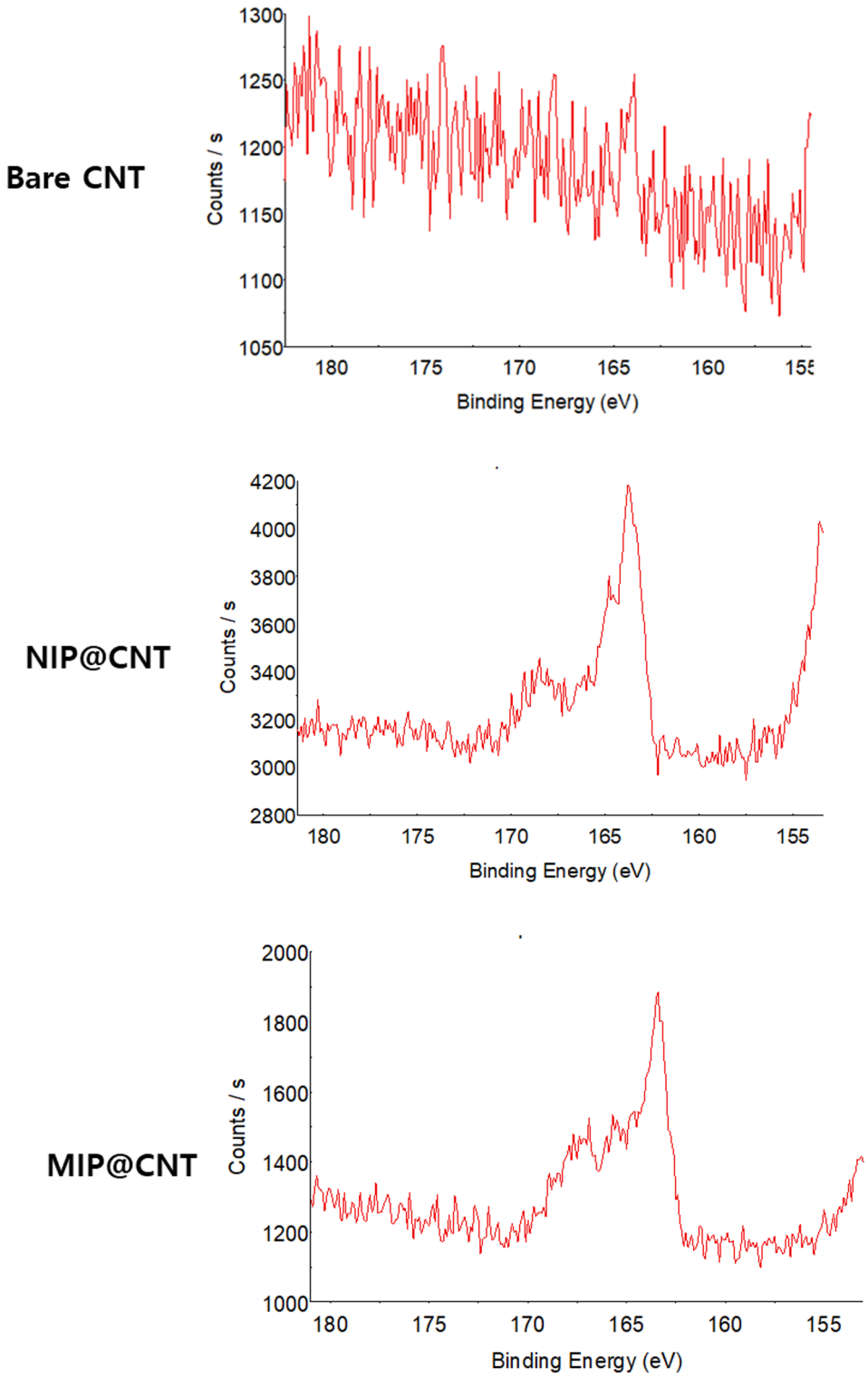

Fig. 4. S 2p scan of X-ray photoelectron spectroscopy (XPS). The thiol-ene click reaction on CNT was confirmed by the observation of S 2p in the NIP@CNT and MIP@CNT.

modified chip showed the highest I_p (~ ±150 µA), while NIP@CNT displayed an intermediate I_p (~ ±100 µA), suggesting that the non-imprinted polymer layer partially hindered the redox reaction observed at the bare CNT surface. The MIP@CNT exhibited the lowest peak currents (~ ±50 µA), suggesting that the MIP layer further limited the transport of redox species to the electrode surface. This lower current is attributed to the successful imprinting process, where the recognition cavities captured or interacted with species, thereby slowing the diffusion of the redox mediator, $Fe[(CN)_6]^{3-/4-}$, to the electrode surface.

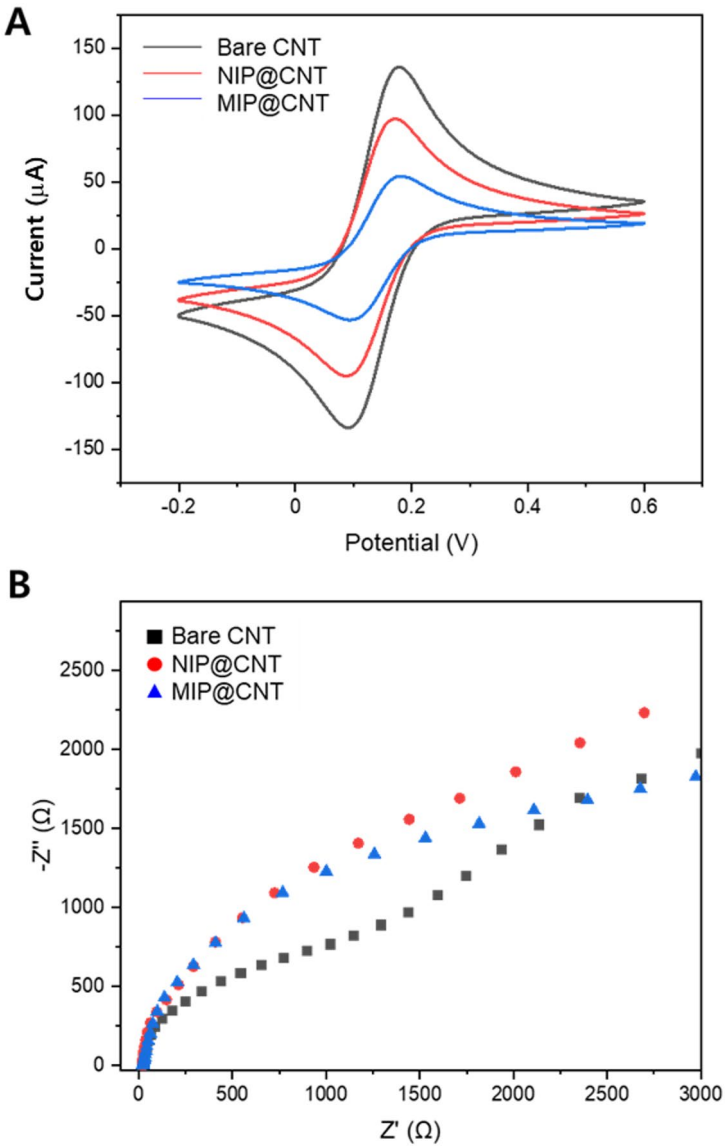

Fig. 5. Electrochemical responses of bare CNT, NIP@CNT, and MIP@CNT-modified SPE chips measured in 0.1× PBS containing 0.1% DMSO. Changes in electrochemical properties of SPE chips after polymer modification. (**A**) Capacitance-voltage (CV) curves. (**B**) Electrochemical impedance spectroscopy (EIS) curves.

Figure 5B displays the Nyquist plot obtained from the EIS measurement. The real axis (*Z'*) represents the fundamental resistance, while the imaginary axis (*-Z"*) shows the capacitive behavior. In the Nyquist plot, the diameter of the semicircle corresponds to the charge transfer resistance (R_{ct}). Figure 5B illustrates that the bare CNT sensor has the lowest R_{ct} (985), indicating the highest electron transfer efficiency. Chips modified with NIP@CNT and MIP@CNT exhibited larger semicircles, resulting in increased R_{ct} values of 2514 and 2575, respectively. This increase is primarily due to the polymer layers acting as barriers to electron transfer. Although MIP@CNT showed a slightly higher R_{ct} than NIP@CNT, the difference was minimal. The overall shape of the EIS curves, specifically the linear-like lines at lower frequencies (known as Warburg impedance), suggests that the sensing process was diffusion-limited. The enhanced Warburg element observed in the curves for NIP@CNT and MIP@CNT helps explain the significant difference in I_p compared to the bare CNT, reflecting their sensitivity to the charge diffusion kinetics of the redox species. The application of the polymer layers to the CNTs serves as a physical barrier that slows the diffusion of the redox mediator, which, in turn, results in the observed decrease in peak current in the CV curves (Fig. 5A). In summary, both NIP@CNT and MIP@CNT introduced polymer-induced resistance in charge transfer on the electrodes compared to the bare CNT-modified chip. For the MIP@CNT sensor, the lowest I_p appears to result from successful imprinting, as the ergosterol recognition sites created in the polymer capture ions or charges, thereby slowing down diffusion onto the chip surface. Similar results, including decreased I_p and increased R_{ct}, have been reported for MIP-based electrochemical sensors[24].

Determination of binding signals from MIP@CNT sensor

To assess the binding capacity of ergosterol to the MIP@CNT sensor, the SWV signal was measured as a function of ergosterol concentration. Figure 6A and B, and 6C illustrate the changes in SWV signals for the bare CNT, NIP@CNT, and MIP@CNT sensors, respectively. When solutions containing 0, 0.1, 1, and 10 pg/mL of ergosterol were applied to the working electrodes of bare CNT sensors, the SWV signal showed a decreasing trend (Fig. 6A). This decrease was attributed to the reduced conductivity of the bare CNT due to its interaction with ergosterol, which resulted in an increased impedance of the redox reaction. Conversely, when the electrodes were modified with NIP@CNT, the SWV signals did not change significantly with the addition of ergosterol (Fig. 6B). This suggests that the NIP forms an insulating layer on the CNT surface, effectively blocking the ionic diffusion or conductivity changes that the ergosterol-CNT interaction causes in the bare CNT, thereby maintaining the electrolyte diffusion to the redox mediator. In the case of NIP@CNT, charge diffusion facilitated by ergosterol binding was unlikely, resulting in minimal changes in the SWV signal compared to the MIP@CNT sensor.

In contrast, ergosterol increased the current in SWV measurements for the MIP@CNT sensors (Fig. 6C). This was interpreted as the ergosterol-MIP interaction at the binding cavity facilitating charge transfer or ionic flow to the mediator through an induced redox reaction. Although ergosterol is a neutral and highly hydrophobic substance, it contains a hydroxyl group capable of interacting with the carbonyl groups of EGDMA. Ergosterol binding may alter the microenvironment at the recognition sites, thereby boosting charge transfer pathways. Since ergosterol binding to the MIPs did not involve direct ionic interactions, it might replace protons or other ionic buffer molecules at the binding sites, which then induces electron diffusion to the redox mediator and causes an increase in the SWV signal. Therefore, the net current change in the NIP@CNT and MIP@CNT sensors was normalized to account for the decreased ionic conductance observed in bare CNTs upon ergosterol addition. In Figure S3, a proposed reaction mechanism for the enhanced charge transfer via ergosterol binding is illustrated.

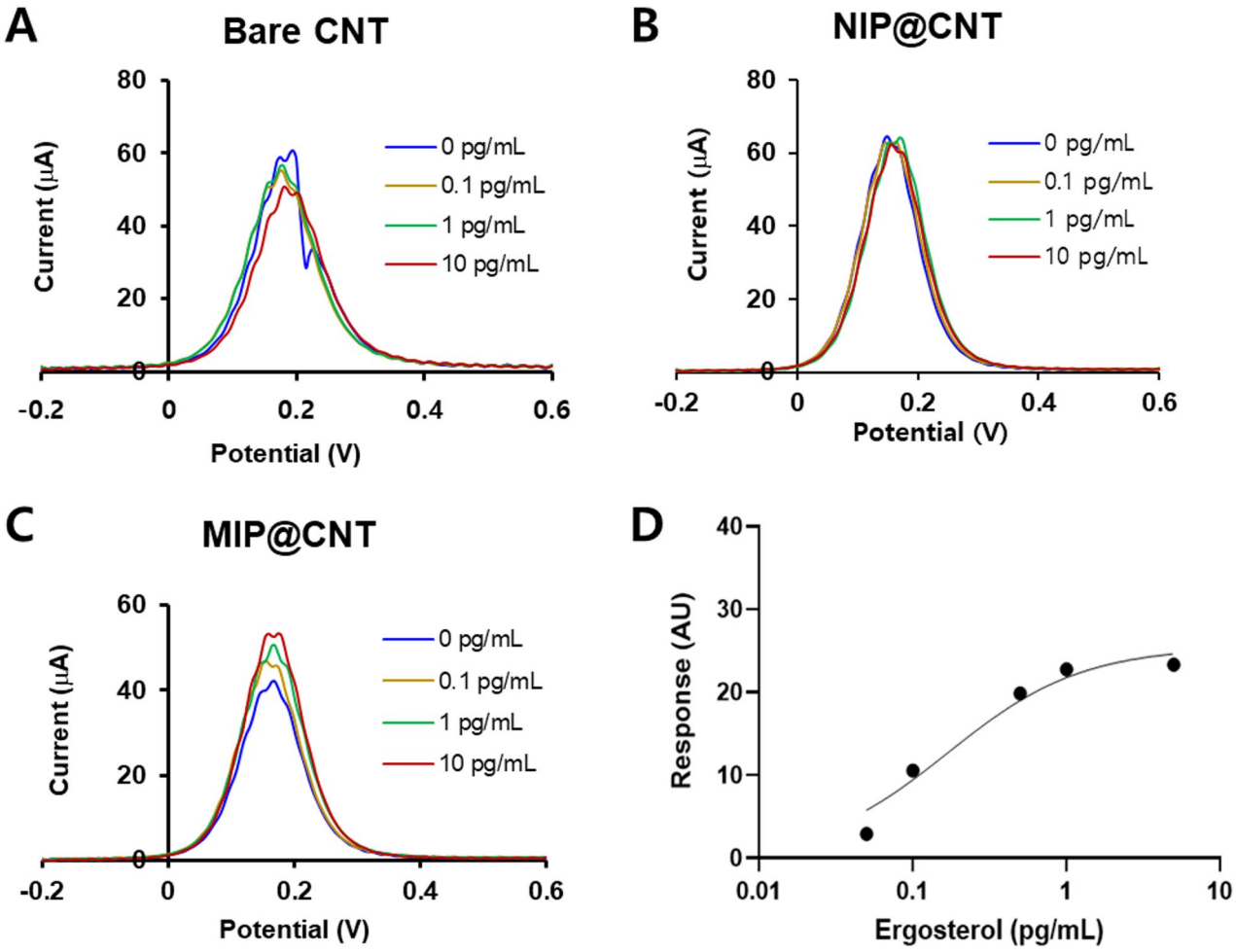

Fig. 6. Measurement of the binding signals for ergosterol at different concentrations (0–100 pg m/L) after 10 min incubation at 37 °C in 0.1× PBS containing 0.1% DMSO. Concentration-dependent SWV curves on (**A**) bare CNT, (**B**) NIP@CNT, and (**C**) MIP@CNT modified SPE sensor. (**D**) Standard curve of ergosterol binding after the normalization of the response ($R^2 = 0.9588$).

While many MIP-based electrochemical sensors exhibit signal suppression due to partial blocking of electron transfer, signal enhancement has also been reported in MIP systems similar to this study. For example, Amatatongchai et al.[25] reported enhanced electrochemical signals for 3-nitrotyrosine (3-NT) and 4-nitroquinolin-N-oxide (4-NQO) dual-MIP sensing system due to improved surface area and electron-transfer properties of the MIP layer. Likewise, MIP-based trazodone sensors have shown signal amplification effects by facilitated charge transfer between the recognition layer and the electrode surface[26].

The sensing response values were calculated by subtracting the current changes observed in bare CNT sensors from those in the NIP@CNT and MIP@CNT sensors at the same ergosterol concentration, which accounts for the inherent decrease in conductivity resulting from the ergosterol-CNT interaction. Finally, the response of the ergosterol sensors was calculated according to Eq. (1) in Sect. 2.4. Figure 6D shows the standard curve of the ergosterol binding response for the MIP@CNT sensor, which exhibits a strong curve fit ($R^2 = 0.9588$).

Determination of imprinting factor, limit of detection, and binding constant

Figure 7A illustrates the concentration-dependent binding response of the NIP@CNT and MIP@CNT sensors, calculated according to Eq. (1) and based on three repeated tests. The binding signal for the NIP@CNT (R_{E_NIP}) was minimal compared to that of the MIP@CNT (R_{E_MIP}) sensor. Figure 7A also shows the inter-electrode reproducibility of the MIP@CNT sensor. The current responses obtained from independently prepared MIP@CNT sensors were consistent, with relatively small variation, indicating good reproducibility in sensor fabrication and stable sensing performance.

The Imprinting Factor (IF), calculated by dividing the binding capacity of the MIPs by that of the NIP at each concentration (R_{E_MIP}/R_{E_NIP}), was determined to be 19.26 at 1 pg/mL and 3.68 at 5 pg/mL ergosterol. Previous reports on ergosterol MIPs showed lower imprinting factors, such as 2.8 for isolating ergosterol from

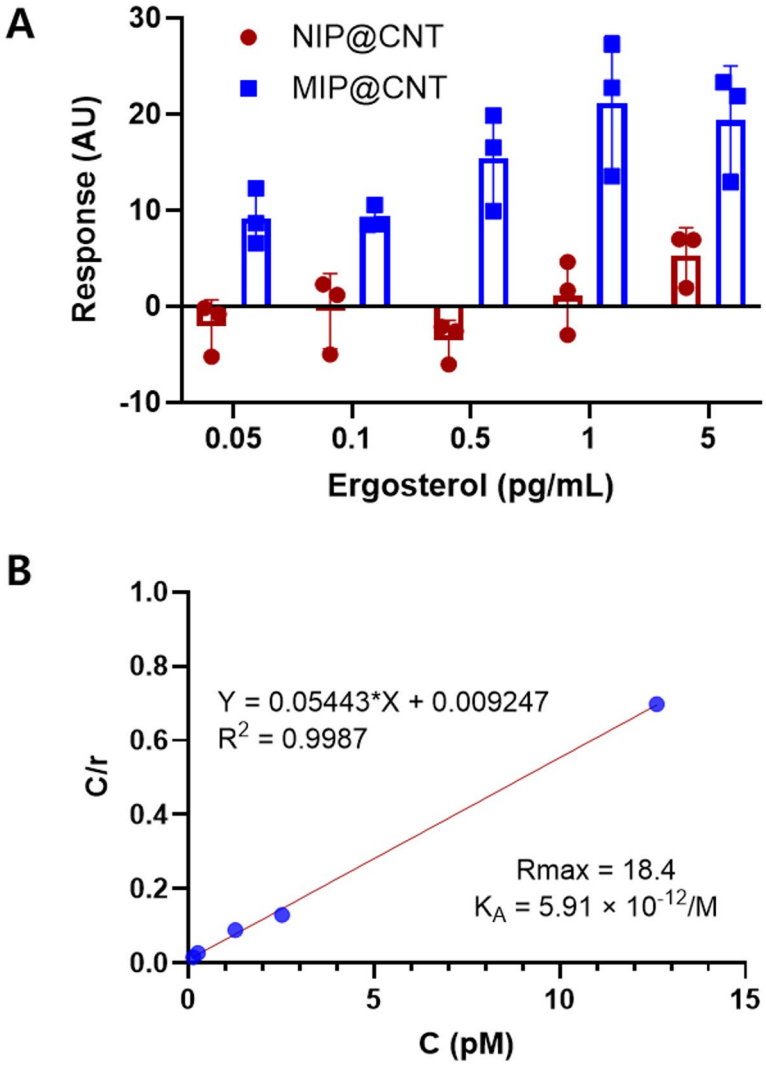

Fig. 7. Binding capacity of ergosterol to MIP@CNT sensor in 0.1× PBS containing 0.1% DMSO at 37 °C. (**A**) Repetitive binding experiment of ergosterol to NIP@CNTs and MIP@CNTs ($n = 3$). (**B**) C vs. C/r curve according to the Langmuir equation to determine the binding constant, K_A.

Ganoderma tsugae[27] and 4.96 for detecting ergosterol from *Aspergillus niger*[28]. In both cases, rebinding was performed using a batch method, involving the incubation of MIP particles with ergosterol for 12 h and 2 h, respectively. Therefore, a direct comparison of binding capacities with previous ergosterol studies is limited by the differing experimental conditions.

Due to the limited available literature on electrochemical ergosterol detection, the performance of our MIP@CNT sensor was compared with several recent cholesterol-detecting electrochemical sensors in Table 1. For MIP-based cholesterol detection, the IF for electrochemical responses typically ranges from 3 to 8.4. Taken together, the binding capacity of the MIP@CNT sensor developed in this study was enhanced compared to that of previous MIP probes for similar sterol-like compounds.

The LOD of the MIP@CNT sensor was determined to be 0.087 pg/mL (0.22 pM), corresponding to a signal of three standard deviations (3 × SD) from three repetitive measurements at 5 pg/mL ergosterol, based on the regression curve in Fig. 6D. In comparison, aptamer-based electrochemical sensors for other fungal mycotoxins have been reported to be 0.12 pg/mL LOD for ochratoxin A at concentrations ranging from 0.12 pg/mL to 5.5 pg/mL (Rhouati et al., 2016) and 1.15 pg/mL LOD for aflatoxin B at concentrations ranging from 2 pg/mL to 150 pg/mL using EIS analysis[29]. In addition, the LODs for cholesterol MIP sensors have been reported in wide ranges from 2.39 fM to 0.85 mM, as shown in Table 1.

Taken together, the MIP@CNT sensor for ergosterol yielded low LOD values that was comparable to, or improved upon, those of previously developed aptamer-based mycotoxin sensors and MIP-based cholesterol sensors. These results suggest that the MIP@CNT probes offer a promising sensing material for the detection of ergosterol.

The Langmuir isotherm equation was used to determine the binding constant of ergosterol to the MIP@CNT sensor. Although the Langmuir isotherm model has been reported to sometimes be unsuitable for ligand-receptor adsorption in proteins[30], it remains the preferred choice for MIP-based biosensors[31]. This preference is due to the model's assumptions—non-cooperative and equilibrium binding in a macroscopic ensemble—which align well with the characteristics of MIPs as synthetic, non-biomolecular probes for small molecule ligands. Consequently, the Langmuir isotherm has been applied to MIP-based biosensors, including those utilizing field-effect transistors (FET)[32], electrochemical sensors[33], and gold nanoparticle-decorated SPE sensors[34]. The plot of the Langmuir isotherm, showing concentration (C) versus concentration divided by response (C/r) according to Eq. (2) in "Determination of the binding constant of ergosterol to the MIP@CNT sensor" section, is presented in Fig. 7B based on three repeated measurements. The association constant (K_A) of ergosterol binding to MIP@CNT was calculated as 5.88×10^{12} M^{-1}, and the dissociation constant (K_D) was found to be 1.70×10^{13} M by inverting the K_A. The maximum response value (R_{max}) derived from the parameter (1/a) of the curve fit in Fig. 7B was 18.4. These quantitative parameters (IF, LOD, and binding constant) demonstrated that the ergosterol probes were successfully prepared for MIP@CNT sensor to exhibit enhanced sensing capabilities for ergosterol.

The association constant estimated from the Langmuir fitting should be interpreted as an apparent binding affinity. The Langmuir model assumes homogeneous binding sites and monolayer adsorption; however, MIPs typically possess heterogeneous binding sites with a distribution of affinities. The fitted parameters from this study primarily reflect the dominant binding contribution of high-affinity sites rather than a strict thermodynamic equilibrium constant. Previous studies have reported that MIP-based sensing systems can exhibit very strong apparent binding affinities comparable to those of antibody–antigen interactions, particularly when optimized imprinting strategies are employed. For example, nanoMIP-based sensors have demonstrated dissociation constants in the picomolar range, corresponding to association constants approaching 10^{11}–10^{12} M^{-1}, highlighting the possibility of extremely strong template–probe interactions in well-designed imprinted systems[35].

At the same time, it is recognized that overestimation of binding constants may occur when Langmuir fitting is applied to heterogeneous systems or when the sensor response approaches saturation at very low analyte concentrations, which can bias the fitted parameters toward higher apparent affinities. Therefore, the association

No.	MIP composition	Sensing platform	MIP immobilization	Detection method	LOD	Imprinting factor (IF)	Reference
1	[2-(dimethylamino) ethyl methacrylate]	Pencil graphite electrode	Electro-polymerization	Electrochemical DPV signal	0.85 mM	3.36	Dianovita et al. (2025)[36]
2	Styrene/divinylbenzene composites with Ag@MoO_3 nanorods	Silver-finished interdigital capacitors	In situ polymerization by AIBN	Capacitance using LCR meter	0.03 µM	3.78	Ejaz et al. (2025)[37]
3	MMA/EGDMA	PCB microchip	UV irradiation	Capacitance using LCR meter	0.31 mM	~ 3[a)]	Hayat et al. (2024)[38]
4	[3-(triethoxysilyl)propyl isocyanate] composites with Fe_3O4/SiO_2	Magneto graphite-epoxy composite electrode	Adsorption to electrodes	Electrochemical SWV signal	0.15 µM	-	Peixoto Lins et al. (2023)[39]
5	Hollow carbon spheres and 2-(perfluorohexyl) ethyl methacrylate	Perovskites on ITO	Adsorption to electrodes	Photoelectrochemical photocurrent change	2.39 fM	~ 8.4[a)]	Yu et al. (2023)[40]
6	MMA/EGDMA/GO	CNT-deposited screen-printed electrode	PETMP/GO thiol-ene click reaction to CNT by UV irradiation	Electrochemical SWV signal	0.22 pM	19.3	This work

Table 1. Comparison of binding properties for cholesterol to its MIP probes and this work with electrochemical sensor platforms. a) Calculated using the data and charts provided in the literature.

constant reported in this study should be considered an apparent parameter describing the binding behavior of the imprinted sensor rather than a strict thermodynamic value.

Evaluation of competitive binding

To ensure the utility of the MIP@CNT as a probe for ergosterol, it must be capable of discriminating between ergosterol and structurally similar molecules. In this study, we investigated the binding capacity of β-sitosterol, stigmasterol, and cholesterol, which share similar structures and molecular weights with ergosterol. β-Sitosterol is a common plant sterol found in various foods, such as nuts, seeds, and vegetable oils, while stigmasterol is another phytosterol abundantly found in plants. As shown in Fig. 8A and B, and 8C, neither competitor sterol produced a clear electronic signal on the MIP@CNT sensor.

The bar graph (Fig. 8D) summarizing the current changes further highlights the sensor's selectivity, with ergosterol generating the largest signal response among the sterol analogues. This difference can be attributed to the specific molecular imprinting process, which creates binding cavities complementary to the size, shape, and functional groups of ergosterol. Although the tested sterols possess similar steroid ring structures, subtle differences in their side-chain configurations reduce their binding affinity to the imprinted sites. These results strongly suggest that the molecularly imprinted cavities in the MIP@CNT probes were successfully optimized to selectively recognize and bind ergosterol while effectively excluding its structural analogs.

Optimization of binding site regeneration and ergosterol binding conditions for MIP@CNT

After the imprinting process is complete, the binding sites are occupied by the ergosterol template. For the probe to be reused, these binding sites must be regenerated by effectively removing the ergosterol template. The regeneration procedure involved washing the MIP@CNT product with absolute ethanol coupled with sonication. To optimize this process, the sonication time was adjusted to achieve the best subsequent rebinding performance.

Figure 9 shows the time-dependent SWV signals after 0, 15, and 30 min of sonication of the MIP@CNTs in absolute ethanol (Fig. 9A and B, and 9C). The net current changes observed upon rebinding with 0.1 ng/mL ergosterol increased to a maximum after 15 min of sonication (Fig. 9D). As a result, 15 min was selected as the optimized sonication time for effectively regenerating the binding sites.

When the sensor was subjected to sequential measurements of background signals, the overlaid voltammetric curves showed that although the general peak position was maintained, peak intensity varied after repeated cycles (Figure S1). This signal variation is likely due to partial changes in the sensing surface of the MIP@CNT

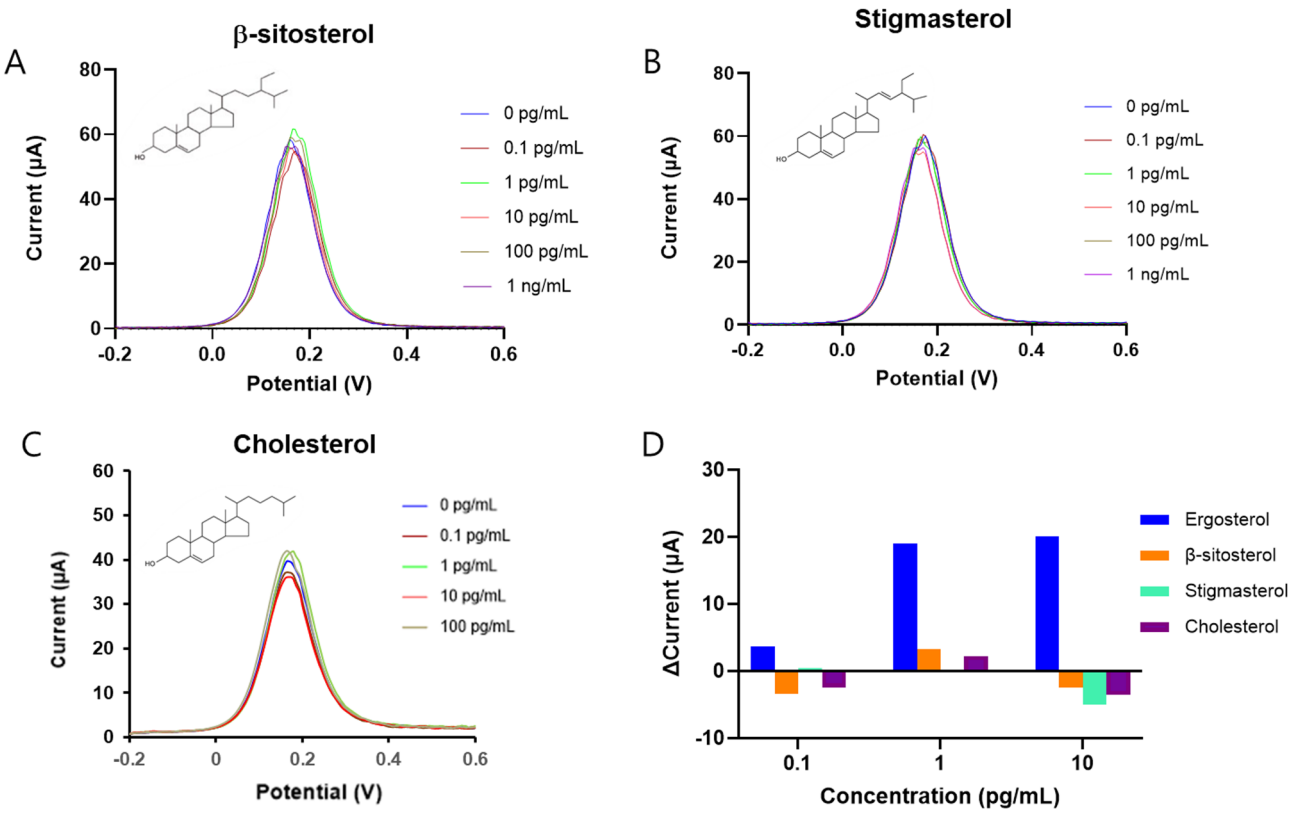

Fig. 8. Competitive binding property for MIP@CNT sensor measured by SWV after 10 min incubation at 37 °C in 0.1× PBS containing 0.1% DMSO. (**A**) β-sitosterol. (**B**) Stigmasterol. (**C**) Cholesterol. (**D**) Comparison of ergosterol, β-sitosterol, stigmasterol, and cholesterol to the MIP@CNT sensor. ΔCurrent was calculated by the subtraction of the peak current at zero pg/mL from the peak current for each concentration of sterols.

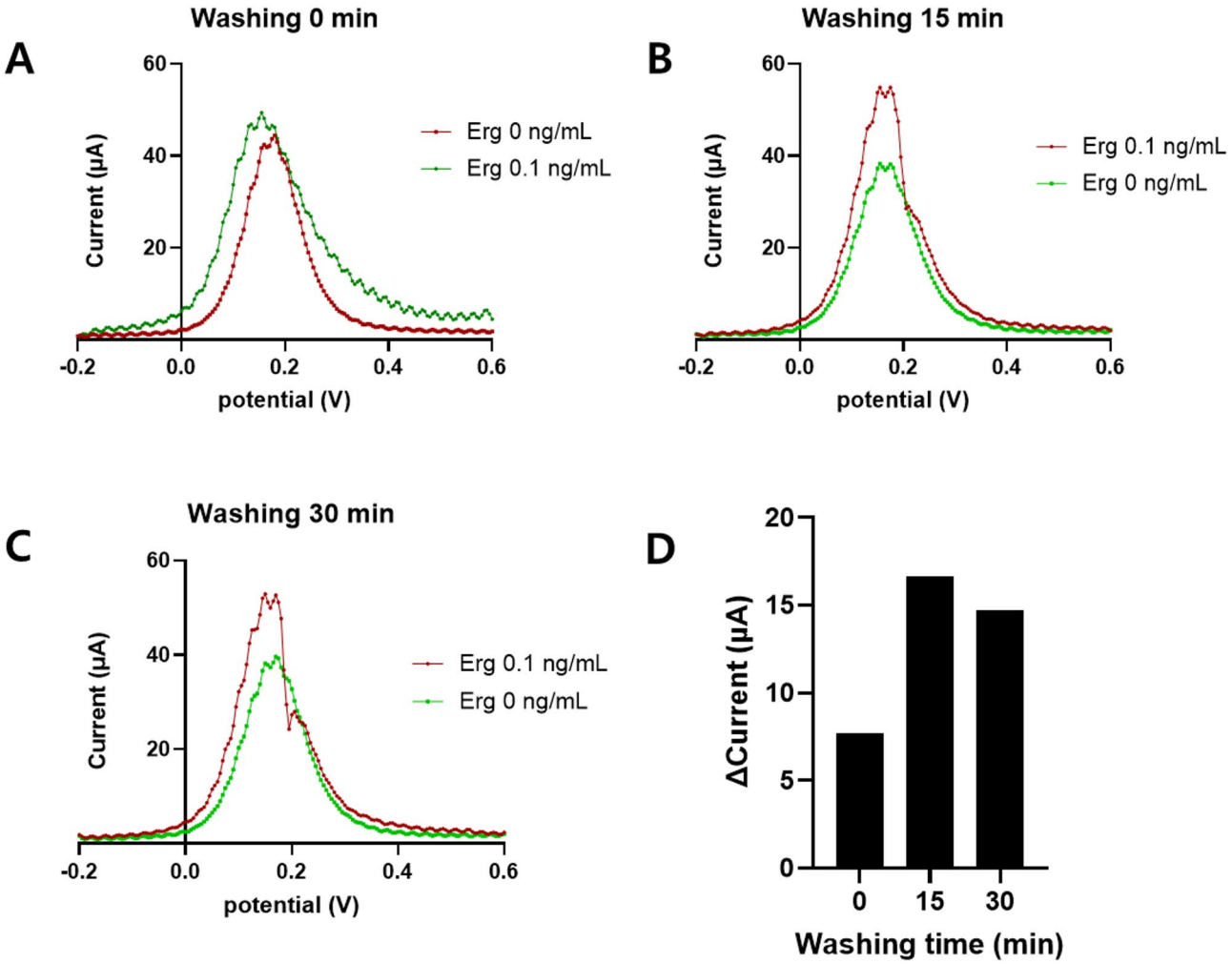

Fig. 9. Optimization of washing time for regenerating ergosterol binding sites on MIP@CNT sensors. Square wave voltammetry (SWV) responses were measured toward ergosterol under different washing conditions. Red and green curves represent measurements before and after ergosterol binding, respectively. All measurements were performed in 0.1× PBS containing 0.1% DMSO after incubation for 10 min (**A**), 15 min (**B**), and 30 min (**C**) at 37 °C. (**D**) Comparison of the current changes under three different washing time conditions.

sensor during current-voltage application. These results indicate that the MIP@CNT sensor is more suitable for single-use sensing applications, which is consistent with the disposable nature of screen-printed electrode platforms.

To optimize the sensing performance of the MIP@CNT sensor, the effects of incubation temperature and incubation time on the electrochemical response were investigated. Two temperatures (27 °C and 37 °C) and four incubation times (1, 5, 10, and 30 min) were evaluated. As shown in Figure S4, the current response increased with incubation time from 1 to 10 min, indicating increased binding of ergosterol molecules to the imprinted recognition sites. However, further extending the incubation time to 30 min resulted in only minor changes in the signal, suggesting that the adsorption process approached equilibrium after approximately 10 min. In addition, the sensor exhibited slightly higher current responses at 37 °C than at 27 °C, which may be attributed to enhanced molecular mobility and faster interactions between ergosterol and the imprinted cavities at elevated temperature. Therefore, 37 °C with a 10-minute incubation time was selected as the optimal condition for subsequent electrochemical measurements.

Determination of ergosterol concentration for the monitoring of bio-contaminants in indoor air

The ergosterol concentrations in indoor air samples were quantified using both conventional GC/MS analysis and the MIP@CNT sensor. To enable direct comparison, GC/MS analysis was conducted on the same set of air samples collected at identical sampling sites. The relationship between ergosterol concentrations measured using the MIP@CNT sensor and those obtained by GC/MS was evaluated using Pearson correlation analysis. The statistical significance of the correlation was expressed using the *p*-value, confirming a meaningful correlation between the two analytical methods. A regression model was applied to visualize the relationship between the

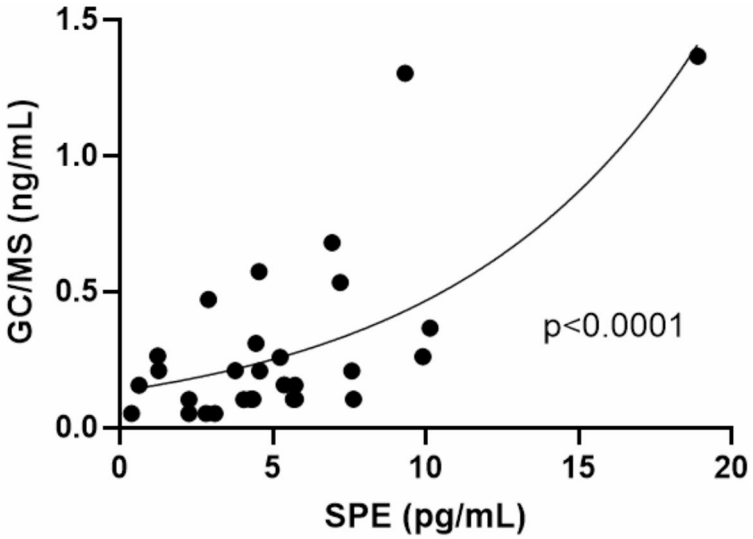

Fig. 10. Comparison of ergosterol concentration in indoor air samples measured by MIP@CNT sensors and GC/MS analysis ($n = 30$). The solid line represents linear regression ($R^2 = 0.5136$), and statistical significance was evaluated using Pearson correlation analysis (p-value).

datasets. As shown in Fig. 10, the two methods exhibited a statistically significant correlation ($p < 0.0001$), with a regression R^2 value of 0.5136.

Despite the significant correlation, the concentrations measured by the MIP@CNT sensor were approximately one to two orders of magnitude lower than those obtained via GC/MS. This discrepancy can be attributed to the extremely low aqueous solubility of ergosterol (≈a few μg/L in pure water without surfactants or organic solvents). In GC/MS, samples were extracted using hexane, which efficiently dissolves ergosterol from PVC filters, allowing measurement of the majority of ergosterol due to its lipophilic nature. In contrast, the MIP@CNT sensor operates on a gold SPE platform restricted to aqueous environments. Consequently, only the fraction of ergosterol that partitioned into the aqueous phase after bead beating was detectable by the sensor, leading to reduced apparent concentrations compared to GC/MS. Importantly, this difference does not indicate functional shortcomings of the sensor. Rather, it reflects distinct chemical environments inherent to each technique: GC/MS captures both soluble and lipophilic extractable fractions, while the MIP@CNT sensor quantifies only the water-soluble and diffusible portion.

Future work is required to establish conversion or compensation strategies to better align sensor-based results with the absolute ergosterol content. To improve the quantitative accuracy of the sensor toward total ergosterol content, several strategies could be considered. By introducing low concentrations of surfactants or small fractions of organic solvents (e.g., ethanol or methanol), the extraction efficiency could be enhanced, which increases ergosterol solubility while maintaining compatibility with the MIP recognition sites and electrochemical measurements. In addition, empirical calibration models correlating electrochemical signals with GC/MS-derived total ergosterol concentrations could be established, allowing the sensor to provide more accurate estimations of fungal biomass in environmental samples.

The MIP@CNT sensor remains a promising tool for rapid, on-site bio-contaminant monitoring, offering real-time detection with reduced labor, time, and cost. The enhanced sensitivity, low LOD, and strong binding affinity of the MIP@CNT sensor support its feasibility for measuring ergosterol in indoor air samples using simple aqueous extraction methods.

Conclusion

This study introduces an enhanced analytical approach for ergosterol detection that can complement or potentially replace conventional techniques, providing a practical and efficient platform for environmental monitoring. As ergosterol is a key biomarker of airborne fungal contamination, its detection in air samples is critical for evaluating indoor air quality and assessing potential health risks from fungal exposure. The MIP@CNT probes demonstrated in this study show strong potential for broader applications, including monitoring of fungal contamination in water, food, and other environmental samples.

In summary, a CNT-supported MIP sensor based on PETMP–GO dual anchoring chemistry was developed for the electrochemical detection of ergosterol. This design promotes efficient interaction between the imprinted recognition sites and target molecules, providing a promising approach for constructing selective and sensitive MIP platforms. However, long-term storage stability was not systematically investigated in this study and remains a subject for future work.

Given the growing interest in MIP-based detection systems, this work may serve as a reference for developing sensing platforms targeting highly hydrophobic biomolecules such as cholesterol and phytosterols, which require rapid, convenient detection methods for diverse environmental and public health applications.

Data availability

The datasets generated and analyzed during the current study are available from the corresponding author upon reasonable request.

Received: 3 November 2025; Accepted: 1 April 2026
Published online: 10 April 2026

References

1. Lindemann, V. et al. Analysis of mold and mycotoxins in naturally infested indoor building materials. *Mycotoxin Res.* **38**, 205–220. https://doi.org/10.1007/s12550-022-00461-3 (2022).
2. Ghanbarian, M., Ghanbarian, M., Ghanbarian, M., Mahvi, A. H. & Hosseini, M. Determination of bacterial and fungal bioaerosols in municipal solid-waste processing facilities of Tehran. *J. Environ. Health Sci. Eng.* **18**, 865–872. https://doi.org/10.1007/s40201-020-00510-y (2020).
3. Alba-Mejía, J. E. et al. Ergosterol and polyphenol contents as rapid indicators of orchardgrass silage safety. *Heliyon* **9**, e14940 https://doi.org/10.1016/j.heliyon.2023.e14940 (2023).
4. Adamczyk, S., Lehtonen, A., Mäkipää, R. & Adamczyk, B. A step forward in fungal biomass estimation – a new protocol for more precise measurements of soil ergosterol with liquid chromatography-mass spectrometry and comparison of extraction methods. *New. Phytol.* **241**, 2333–2336. https://doi.org/10.1111/nph.19450 (2014).
5. Douglas, L. M. & Konopka, J. B. Fungal membrane organization: The eisosome concept. *Annu. Rev. Microbiol.* **68**, 377–393. https://doi.org/10.1146/annurev-micro-091313-103507 (2014).
6. Rodrigues, M. L. The multifunctional fungal ergosterol. *mBio* **9**, e01755–e01718. https://doi.org/10.1128/mbio.01755-18 (2018).
7. Gutarowska, B., Skóra, J. & Pielech-Przybylska, K. Evaluation of ergosterol content in the air of various environments. *Aerobiologia (Bologna)*. **31**, 33–44. https://doi.org/10.1007/s10453-014-9344-4 (2015).
8. Bajzát, J. et al. Development of a simple HPLC method for the analysis of ergosterol and UV-enriched vitamin D_2 in mushroom powders. *Appl. Sci.* **15**, 4058. https://doi.org/10.3390/app15074058 (2025).
9. Kozajda, A. I., Jeżak, K., Sowiak, M., Gutarowska, B. & Szadkowska-Stańczyk, I. Assessment of exposure to fungi in the heavily contaminated work environment (a solid waste sorting plant) based on the ergosterol analysis. *Int. J. Occup. Med. Environ. Health*. **28**, 813–821. https://doi.org/10.13075/ijomeh.1896.00455 (2015).
10. Kadam, U. S. & Hong, J. C. Advances in aptameric biosensors designed to detect toxic contaminants from food, water, human fluids, and the environment. *Trends Environ. Anal. Chem.* **36**, e00184. https://doi.org/10.1016/j.teac.2022.e00184 (2022).
11. Jaoued-Grayaa, N., Nasraoui, C., Chevalier, Y. & Hbaieb, S. Design of molecularly imprinted polymer materials relying on hydrophobic interactions. *Colloids Surf. A: Physicochem Eng. Aspects*. **647**, 129008. https://doi.org/10.1016/j.colsurfa.2022.129008 (2022).
12. Vasapollo, G. et al. Molecularly imprinted polymers: Present and future prospective. *Int. J. Mol. Sci.* **12**, 5908–5945. https://doi.org/10.3390/ijms12095908 (2011).
13. Becskereki, G., Horvai, G. & Tóth, B. The selectivity of molecularly imprinted polymers. *Polymers* **13**, 1781. https://doi.org/10.3390/polym13111781 (2021).
14. Kadhem, A. J., Gentile, G. J. & de Fidalgo, M. M. Molecularly imprinted polymers (MIPs) in sensors for environmental and biomedical applications: A review. *Molecules* **26**, 6233. https://doi.org/10.3390/molecules26206233 (2021).
15. Hassan, R. A., Abu Hanifah, S. & Heng, L. Y. Advancements and prospects of molecularly imprinted polymers as chemical sensors: A comprehensive review. *Talanta* **287**, 127592. https://doi.org/10.1016/j.talanta.2025.127592 (2025).
16. Wei, G. et al. Molecularly imprinted polymer-based system for simultaneous fluorescence quantification of malachite green and crystal violet. *Microchim. Acta*. **192**, 626. https://doi.org/10.1007/s00604-025-07465-7 (2025).
17. Song, Z. et al. Lateral flow chromatography strip system for rapid fluorescence determination of phycocyanin in water samples. *J. Hazard. Mat.* **480**, 135927. https://doi.org/10.1016/j.jhazmat.2024.135927 (2024).
18. Zhang, Y. et al. Facile fluorescence detection of malachite green in fish using molecularly imprinted polymers doped CdTe quantum dots based system. *Food Chem.* **442**, 138458. https://doi.org/10.1016/j.foodchem.2024.138458 (2024).
19. Feng, W. et al. Durable and highly signal-stable pressure sensors prepared by sequential thiol-acrylate click reactions. *Chem. Eng. J.* **493**, 152749. https://doi.org/10.1016/j.cej.2024.152749 (2024).
20. Chen, S. et al. Load transfer of thiol-ended hyperbranched polymers to improve the strength and longation of CNTs/epoxy nanocomposites. *Eur. Polym. J.* **120**, 109254. https://doi.org/10.1016/j.eurpolymj.2019.109254 (2019).
21. Ishikawa, K. et al. Surface sulfurization of amorphous carbon films in the chemistry of oxygen plasma added with SO2 or OCS for high-aspect-ratio etching. *Appl. Surf. Sci.* **645**, 158876. https://doi.org/10.1016/j.apsusc.2023.158876 (2024).
22. Saxena, K. et al. Fabrication of a molecularly imprinted nano-interface-based electrochemical biosensor for the detection of CagA virulence factors of H. pylori. *Biosens. (Basel)*. **12**, 1066. https://doi.org/10.3390/bios12121066 (2022).
23. Rosario, W., Avasthi, D. K. & Chauhan, N. Graphene oxide and molecularly imprinted polymer-based sensor for the electrochemical detection of benzene: A novel tactic in early diagnosis of lung cancer. *Talanta Open.* **12**, 100506. https://doi.org/10.1016/j.talo.2025.100506 (2025).
24. Lian, W., Zhang, X., Han, Y., Li, X. & Liu, H. A molecularly imprinted electrochemical sensor for carbendazim detection based on synergy amplified effect of bioelectrocatalysis and nanocomposites. *Polymers* **17**, 92. https://doi.org/10.3390/polym17010092 (2025).
25. Amatatongchai et al. Facile and compact electrochemical paper-based analytical device for point-of-care diagnostic of dual carcinogen oxidative stress biomarkers through a molecularly imprinted polymer coated on graphene quantum-dot capped gold. *Anal. Chem.* **94** (48), 16692–16700. https://doi.org/10.1021/acs.analchem.2c03120 (2022).
26. Seguro, I., Rebelo, P., Pacheco, J. G. & Delerue-Matos, C. Electropolymerized, molecularly imprinted polymer on a screen-printed electrode-a simple, fast, and disposable voltammetric sensor for trazodone. *Sens. (Basel)*. **22**, 2819. https://doi.org/10.3390/s22072819 (2022).
27. Hashim, S. N. et al. Recovery of ergosterol from the medicinal mushroom, Ganoderma tsugae var. Janniae, with a molecularly imprinted polymer derived from a cleavable monomer-template composite. *J. Chromatogr. A*. **1468**, 1–9. https://doi.org/10.1016/j.chroma.2016.09.004 (2016).
28. Oktay Başeğmez, H., Baydemir Peşint, G., Nergiz, M. & Zenger, O. Determination of mold contamination using ergosterol imprinted particles. *Biotechnol. Prog.* **37**, e3089. https://doi.org/10.1002/btpr.3089 (2021).
29. Rhouati, A., Catanante, G., Nunes, G., Hayat, A. & Marty, J. L. Label-free aptasensors for the detection of mycotoxins. *Sensors* **16**, 2178. https://doi.org/10.3390/s16122178 (2016).
30. Latour, R. A. The Langmuir isotherm: A commonly applied but misleading approach for the analysis of protein adsorption behavior. *J Biomed. Mater. Res Part A*. **103A**, 949–958. https://doi.org/10.1002/jbm.a.35235 (2015).
31. Zangi, R. Breakdown of Langmuir adsorption isotherm in small closed systems. *Langmuir* **40**, 3350–3356. https://doi.org/10.1021/acs.langmuir.3c03894 (2024).
32. Yang, H. Potentiometric Langmuir isotherm analysis of histamine-selective molecularly imprinted polymer-based field-effect transistor. *ECS J. Solid State Sci. Technol.* **7**, Q3079. https://doi.org/10.1149/2.0131807jss (2018).

33. Esavento, M., Marchetti, S., De Maria, L., Zeni, L. & Cennamo, N. Sensing by molecularly imprinted polymer: Evaluation of the binding properties with different techniques. *Sens. (Basel).* **19**, 1344. https://doi.org/10.3390/s19061344 (2019).
34. Manrique Rodriguez, N. A. et al. Adsorption isotherm analysis for hybrid molecularly imprinted polymeric gold-decorated nanoparticles suitable for reliable quantification of gluconic acid in wine. *Nanomater (Basel).* **15**, 211. https://doi.org/10.3390/nano15030211 (2025).
35. Sehit, E. et al. computationally designed epitope-mediated imprinted polymers versus conventional epitope imprints for the detection of human adenovirus in water and human serum samples. *ACS Sens.* **9**, 1831–1841. https://doi.org/10.1021/acssensors.3c02374 (2024).
36. Dianovita, F. A., Yulianti, E. S., Hanafiah, S. & Rahman, S. F. Molecularly-imprinted polymer based on graphene oxide functionalized pencil graphite electrode for cholesterol detection. *Biochem. Eng. J.* **221**, 109769. https://doi.org/10.1016/j.bej.2025.109769 (2025).
37. Ejaz, K., Akhtar, M., Hussain, T., Mujahid, A. & Afzal, A. Noninvasive cholesterol sensing by poly(styrene-co-divinylbenzene) with Ag@MoO3 nanorods. *Anal. Sens.* **5**, e202500034. https://doi.org/10.1002/anse.202500034 (2025).
38. Hayat, H. et al. Development of cholesterol imprinted polymer-based interfaces as smart sensors for detection of cholesterol in clinical samples. *J. Mater. Res.* **39**, 459–470. https://doi.org/10.1557/s43578-023-01241-0 (2024).
39. Peixoto et al. Development of a bio-inspired magnetic nanocomposite synthesized through semi-covalent imprinting for electrochemical determination of cholesterol in water samples. *Electroanal* **35**, e202300145. https://doi.org/10.1002/elan.202300145 (2023).
40. Yu, L. et al. Molecularly imprinted ultrasensitive cholesterol photoelectrochemical sensor based on perfluorinated organics functionalization and hollow carbon spheres anchored organic-inorganic perovskite. *Biosens. Bioelectron.* **237**, 115496. https://doi.org/10.1016/j.bios.2023.115496 (2023).

Acknowledgements

This work was supported by the Ministry of Environment, Republic of Korea (MOE) (Project No. 2021003370004) and the Ministry of Science and ICT, Republic of Korea (DGIST Basic Program, Project No. 25-IT-03).

Author contributions

E.S. Choi conducted the main experiments and wrote the manuscript. J.H. Kim contributed to data interpretation. Y.C. Na carried out the GC/MS analysis of the air samples. B.G. Lee and M.K. Yeo were responsible for air sample collection. E. Kim conceived and supervised the study and wrote the manuscript.

Funding

This work was supported by the Ministry of Environment, Republic of Korea (MOE) (Project No. 2021003370004) and the Ministry of Science and ICT, Republic of Korea (DGIST Basic Program, Project No. 25-IT-03).

Declarations

Competing interests

The authors declare no competing interests.

Additional information

Supplementary Information The online version contains supplementary material available at https://doi.org/10.1038/s41598-026-47624-1.

Correspondence and requests for materials should be addressed to E.K.

Reprints and permissions information is available at www.nature.com/reprints.

Publisher's note Springer Nature remains neutral with regard to jurisdictional claims in published maps and institutional affiliations.